CHAPTER I
INTRODUCTION AND LITERATURE REVIEW

1.1 History of nanotechnology

Nanotechnology is an emerging area of science which concerns itself with the study of materials that have very small dimensions, in the range of “nano” scale. The word itself is a combination of nano, from the Greek “nanos” (or Latin “nanus”), meaning “Dwarf” and the word "Science" meaning knowledge [1]. Nanoscience has blossomed over the last twenty decades and the need for nanotechnology will only increase as miniaturization becomes more essential areas such as physics, engineering, chemistry, computing, sensors and biomedical applications. Those advances in this field largely depend on the ability to synthesize nanoparticles of various materials, sizes and shapes, as well as efficiently assemble them into complex architectures. The synthesis of nanoparticles, however, is a fairly established field as particles of submicron or nanosized dimensions have been synthesized for centuries. The first example of significant detection is the Roman Lycurgus bronze cup (figure.1.1) lined with colored glass that dates to the fourth Century AD. The glass scatters a dull green light and transmits red light. According to a study specially made by the British Museum, who currently displays the cup, the glass contains 70 nm particles those are an alloy of silver (70%) and gold (30 %) [2]. Silver nanoparticles (Ag NPs) of this size are known to scatter green light and transmit orange and the addition of gold (Au) shifts the absorption band to longer wavelengths. Although this particular application of nanoparticles may be accidental and small, nanoparticles were often used in later centuries to create stained glass with small ruby red Au and lemon-yellow Ag NPs [3]. Richard Feynman in his speech “There's Plenty of Room at the Bottom”, at an American Physical Society meeting in the California Institute of Technology in December 1959 identified the potential of nanotechnology. He said that it should be possible to build machines small enough to manufacture objects with atomic precision and that information could be written on an atomic scale [4]. In 1962, Ryogo Kubo reported that the energy levels of the ultra-tiny metal particles vary from the bulk materials and change with the particle diameters [5]. This interesting phenomenon leads the scientist to pay much attention in researches of

nanoscale materials. In 1974, Norio Taniguchi first used the word "Nanotechnology" in a paper on ion sputter machining. His article describes the "production technology to get the extra-high accuracy and ultra-fine dimensions on the order of one nanometer" [6]. Ever since, the word Nanotechnology has become a proper noun for upcoming generations. In the 1980s, Eric Drexler authored the landmark book on nanotechnology, "Engines of Creation" in which the concept of molecular manufacturing was introduced [7] but there were no instruments that could distinguish the single atom and molecule directly. This publication has not brought any great influence upon the scientific field. G. Binning and C.F. Quate discovered the Scanning tunnelling microscope (STM) and atomic force microscope (AFM) in 1982 and 1986 respectively [8, 9]. They mainly fabricated the surface analysis instrument to observe the single atom and the atomic arrangement successfully. Since, then human beings can observe the materials in ultra-tiny scale and the nanoscale materials were reported by a series of researches one by one. In 1985, Smalley, Kroto and Curl discovered a third major form of elemental carbon which was called buck balls. The new allotrope of carbon is formally identified as fullerenes [10]. In 1993, Iijima described the synthesis methods of single-walled nanotubes (SWNTs) [11]. Nanosized materials are to be an important subject in basic and applied sciences; the unique properties of NPs sparked their application in a broad ranges of different fields including physics, chemistry, biology, material science, medicine, catalysis and so on [12]. The nanoscale materials provide a very exciting research field due to their interesting optical, electronic, magnetic, mechanical and catalytic properties [13-15].

1.2 Nanoscience and nanomaterials

Nanoscience revolution that sprouted throughout the 1990s is having great impact in current and future. It has been established recently as a new interdisciplinary science. It can be defined as an entire knowledge on fundamental properties of nano-size objects [16]. The prefix 'nano' indicates one billionth of a meter or 10^{-9}m. When the size of the materials is reduced to the dimension of 1–100nm, due to large surface to volume ratio, they exhibit properties that are different from their bulk counterparts [17]. In general, materials with at least one dimension below one micron but greater than one nanometer is nanoscale materials. The results of nanoscience are realized in nanotechnology as new materials and functional facilities.

Nanotechnology is based on the manipulation, control and integration of atoms and molecules to form materials, structures, components, devices and systems at the nanoscale, which is the application of nanoscience, especially to industrial and commercial objectives. Due to their small size, nanomaterials exhibit novel properties which largely differ from the bulk materials. The new emergent properties include quantum size effect, nonlinear optical properties and so on. As the result, nanomaterials have extensive applications in civil and industrial areas. For example, they can be used as microelectronic materials, bacteriostatic materials [18] and catalytic materials or magnetic recording materials [19]. They even have potential applications in DNA detection [20] and photo detection [21].

One of the most important features of nanomaterials is that they present great scope to generate a range of nanostructures such as quantum dots, quantum wire, quantum walls, nanotubes, nanobelts, nanoribbons, core-shell structure and their combination, thereby providing great scope for tailoring of physical and chemical properties. While nanomaterials promise great potential for technological applications in daily life, they pose a number of challenges to the scientific community. A physicist has not only to develop characterization techniques to look into the details of the materials at a highly small scale but also needs to develop theories and models towards understanding various mechanisms behind their new and unusual properties. To explain the properties when it is required to go beyond the quantum regime, the engineers have to find the way to handle these tiny particles to integrate them into devices, equipments and system. Though the technology can help the medical science, one has to be highly careful about the harmful effects of these materials and there is need to make in depth toxicity studies on this class of materials. Further, with the rapid growth in the research and application of nanomaterials and nanotechnology there is a strong need to develop standards for their methodology and safe handling. Development of new and novel methods of synthesis to generate the nanomaterials with control on their size, size distribution as well as shape of nanomaterials/nanostructure on a commercial scale with reproducible properties is necessary.

1.3 Top-down and bottom-up approaches

Many different techniques have been developed to generate metal nanoparticles. There are two general strategies to obtain materials on the nanoscale: top-down (physical) and bottom-up (chemical) approaches. The top-down method starts from bulk materials, which are fashioned into nanosized features by carving, milling, etching and patterning. Normally, the physical methods involve costly infrastructure and is ideally suitable to produce material with highly purity and particularly for device applications where small quantities of materials is required. Benefited by increasingly powerful computers, software and well-developed techniques, this method can achieve good control over the device dimension, location and organization with high precision, but high precision induces greater cost when the size of the device is reduced, especially when the size is in nanoscale. On the other hand, chemical methods are preferred to synthesis of nanomaterials in large quantities. In assessment, bottom-up methods construct structures or devices from the basic building blocks, atom by atom or molecule by molecule. This method utilizes the self assembly concept, in which the building blocks, atoms or molecules, automatically arrange themselves in a desired conformation. Bottom-up approaches is usually capable to produce devices in parallel and much cheaper than top-down methods. However, this method could potentially be outgrown as the size and complexity of the desired assembly increases. Sometimes scaling-up can be difficult, for bottom up methods, because both approaches have their own advantages and drawbacks, hybrid methods combining both physical and chemical approaches should be a desired technique in the near future to get molecular resolution and functionality for larger areas [22].

1.4 Type of nanoparticles

Nanoparticles are available with a wide range of morphologies and sates of agglomeration. They include:

- Nanotubes mostly of carbon fullerenes with diameters from 1 to 20nm and length than 1mm.
- Nanowires of metals, semiconductors, etc., comprising a single crystals structure with diameter of 10’s of nanometers and large aspect ratio,

nanocrystals and quantum dots of semiconductor, metals and metal oxides comprising 1000 to 1.00.000 atoms.

- Spherical and dendritic aggregated nanoparticles made from a range of materials including carbon black, fumed silica, metals, metal oxides, ceramics, semiconductors and organic materials. They can range in size from a 10 to 5nm to 100's of nanometers.

- Nanoparticles are very rarely found as single particles and readily form aggregates in which the particles can tightly be bound by covalent held together by relatively weak forces including van der Waals forces.

1.5 Metal nanoparticles

In nanotechnology a particle is defined as small objects that behave as a whole unit in terms of its transport and properties. Particles are classified according to size: in terms of diameter, coarse particles cover a range between 10000 to 2500nm. Fine particles are in range size between 2500 and 100nm. Ultra fine particles or nanoparticles range in size between 100 and 1nm. Nanoparticle of metal with the range of 1-100nm is termed as metal nanoparticles.

Metal nanoparticles (MNPs) are referred to as the particles produced from noble metals which have at least one dimension of the order of 100nm or less, are natural bridges between molecules and extended solids. They are complex, many-electron system, where reduced size and quantum confinement of electrons and phonons give birth to fascinating new effects, with potentially tunable particle size and shape. Owing to their size, nanoparticles have a large surface area than macro-sized materials. The intrinsic properties of metal nanoparticles are mainly determined by size, shape, composition, crystallinity and morphology. Until the beginning of the century, the optical properties of metal particles were invariably studied on large ensembles. Recent progress and interest in optical microscopy has stimulated the study of metal nanoparticles.

1.6 Silver nanoparticles

Metal nanoparticles, especially silver nanoparticles (Ag NPs) have been widely studied because of their unique physical-chemical properties. The most

important feature of silver nanoparticles is the surface Plasmon absorption, which has 10^5-10^6 large excitation cross-sections than ordinary molecular chromospheres and is also more intense than that of other metal particles, due to the weak coupling to inter band transition. The frequency of the silver surface plasmon adsorption can also be tuned from visible to near infrared acting on shape, size or nanoparticles assembly. Ag NPs have high chemical stability and photo stability. Due to the simple surface chemistry of Ag NPs, there has been a progress in the synthesis of Ag NPs with modified shape or size and this offers a range of apparatus with engineering properties, opening the access of nanotechnology. These Ag NPs are building blocks in the 21st century. Silver is a malleable and ductile transition metal with a white metallic cluster appearance. It has high optical reflecting electrical conductivity, thermal conductivity and lowest contact resistance. Silver is one of the noble metal with low reactivity. The bulk form is chemically inert but has high reactivity due to unsaturated baggy bonds on their active surfaces. Ag NPs are one of the promising products in the nanotechnology industry including surface plasmon resonance, fluorescence, Surface Enhanced Raman Scattering (SERS) and photo responsibility, catalytic activities and strong toxicity to micro organisms [23-25]. When the light with a specific wavelength falls on Ag nanoparticles, the conduction electrons on metal surface undergo a collective oscillation known as surface plasmon resonance, which is responsible for the unique optical properties of silver nanoparticles.

1.7 Application of Ag NPs

Ag NPs are being incorporated in plastic, fabrics, and paper, paint and surface coatings. More than 200 products containing Ag NPs are now available for public use [26]. Silver nanoparticles have also been widely exploited for use in photography [27], biosensor [28], as molecular receptor [29], biological labelling [30], catalysis [31], to diagnose certain diseases [32], photonics [33], optoelectronics [34], magnetic [35], semiconductor [36] , nano capacitors [37], SERS [38], drug delivery in cancerous tumours, information storage, formulation of magnetic, cosmetic and beauty application [39]. In the field of chemistry, the Ag NPs are used in fuel cell as electro-catalysis. The most commercialized application of modern metal nanoparticles is utilization of the anti-bacterial property of silver in a variety of products [40]. Silver clusters have been utilized for developing SERS based detection devices that mainly detect biomolecules [41, 42].

1.8 Organic compounds

Carbon-based compounds are considered the fundamental core of organic materials. Organic molecules provide a rich variety of properties, attractive for fundamental investigations in physics, chemistry, biology, engineering and material sciences [43]. Organic compounds constitute a major components of energy source (petroleum, coal, natural gas), food (proteins, fast, carbohydrates, vitamins, hormones, steroids), drug (anaesthetics, antiseptics, antibiotics), material (fibre, fabrics, plastics, paints dyes, soaps, detergent, explosires), plants, insects and shellfish etc., including antiphthisic, antitumor, anti-inflammatory, antimicrobial agents and antimalarial action and can be used for pharmacological treatment of different types of respiratory diseases and especially cancer [44]. AgNPs have been used for millennia in dyeing textiles and manufacturing colorants for painting. The economic push for dyes with high tinting strength, directly related to high extinction coefficients in the visible range, historically led to the selection of substances that could be used at low concentrations. All organic molecules contain carbon (C), virtually all of them contain hydrogen (H) and most contain oxygen (O) and/or nitrogen (N) atoms. Many organic molecules also have halogen atoms such as fluorine (F), chlorine (Cl), bromine (Br), or iodine (I). Other atoms in organic compounds include sulfur (S), phosphorous (P), and even boron (B), aluminium (Al) and magnesium (Mg).

1.9 Background of Raman Scattering

The phenomenon of inelastic scattering of light was first proposed by Smekal in 1923 [45] and was first experimentally observed in 1928 by Indian physicists C. V. Raman and K. S. Krishnan [46, 47] when monochromatic light was scattered from the molecules, scattering process results is two types of scattered light; one of which had the same energy as the incident light and the second one, small fraction of scattered light had different energy. Sir. C. V. Raman was awarded Nobel Prize in Physics for this discovery in 1930.

1.10 Raman Effect

When the energy of the incident light is not large enough to excite the molecule from the ground state to the lowest electronic state, the molecule will be excited to a virtual state between the two states. The electron cannot stay for a long

time in the virtual state and will immediately go back to the ground state. If the electron goes to where it is originated from, then the wavelength of the scattered light is the same as the light source, which is called **Rayleigh scattering**. It is also possible that the electron goes to the vibrational state different from where it is excited and then, there is an energy difference between the emitted photon and the incident photon. If the emitted energy smaller than the incident energy. This process is called **Stokes scattering**. The opposite is called the **Anti-stokes** scattering (Figure.1.2). Raman spectroscopy is an important analytical technique for chemical and biological analysis due to the wealth of information on molecular structures, surface processes and interface reactions that can be extracted from experimental data. The Raman cross section is inherently weak, thus avoids the possibility of achieving low detection limit with normal Raman spectroscopy. However, for the last two decades, Raman techniques have been experiencing increasing application in many fields. This renewed interest in Raman spectroscopy has been due to the observations of enormous Raman enhancement for molecules adsorbed on special metallic surfaces. In 1974, it was first reported that an unusually strong enhanced Raman scattering signal occurred with pyridine molecules adsorbed on silver electrode surfaces that had been roughened electrochemically by oxidation- reduction cycles [48]. The major disadvantage of Raman spectroscopy is that the Raman signals are too weak compared with the intense elastic Rayleigh scattering components, as a result of extreme scattering cross section of Raman process. Hence several schemes have been introduced to overcome this drawback. The most influential among them is SERS. This observation of enhanced Raman signal, originally attributed to a high surface density produced by the roughening of the surface of electrodes, was later determined to be a result of a surface enhancement process, hence the term SERS effect [49, 50]. The enhancement factors for the observed Raman scattering signals of adsorbed molecules were found to be more than a million-fold when compared to normal Raman signals expected from gas phase molecules or from non-adsorbed compounds. This `giant Raman effect' opens a wide spectrum of new possibilities of the Raman technique for trace analysis, chemical analysis, environmental monitoring and biomedical applications.

1.11 Surface Enhanced Raman Scattering (SERS)

1.11.1 *Discovery of Surface-enhanced Raman Scattering*

The name 'SERS' implies that it provides the same information that normal Raman spectroscopy does, simply with a greatly enhanced signal. The weak Raman signal can be greatly enhanced by the introduction of SERS spectroscopy. In 1974, Fleischmann et.al., [47] from the University of Southampton, accidentally discovered this when they tried to do Raman with an adsorbate of very high Raman cross section, such as pyridine (Py) on the roughened silver (Ag) electrode. The initial idea was to generate high surface area on the roughened metal surface. On the basis of their extensive experience in increasing the surface area of an Ag electrode using an electrochemical roughening method, they applied about 450 potential oxidation and reduction cycles (ORC) to an Ag electrode in an aqueous electrolyte comprised of 0.1 mol l^{-1} KCl + 0.05 mol l^{-1} Py. The Raman spectrum obtained of unexpectedly high quality evidently due to the adsorbed Py and the spectra was found to be dependent on the electrode potential. They initially explained that the intense surface Raman signal of Py was due to increased surface area. This was, in fact, the first SERS measurement and the roughened electrode was the first nanostructure exhibiting the SERS activity, although it was not recognized as such in 1974. Later, in 1977, Jeanmaire and Van Duyne from Northwestern University, USA, first realized that surface area is not the main factor in the above phenomenon [48]. Albrecht and Creighton from the University of Kent, UK, reported a similar result in the same year [49]. These two groups provided strong evidences to demonstrate that the strong surface Raman signal must be generated by a real enhancement of the Raman scattering efficiency of surface area (10^5–10^6). The effect was later named as surface-enhanced Raman scattering and now, it is a universally accepted surface sensitive technique. Although the first SERS spectra were obtained from an electrochemical system (Py + roughened Ag electrode), all important reactions on surfaces including electrochemical processes can be studied by SERS. This technique is so sensitive that even a single molecule can be detected. The exact mechanism of the enhancement effect of SERS is still a matter of controversy in the literature. There are two main mechanisms on the large enhancement effect of weak Raman signal from Py adsorbed on electrochemically roughened Ag. Jeanmaire and Van Duyne proposed the theory of electromagnetic effect on the enhancement [48]. The electromagnetic theory is

based on the excitation of localized surface plasmons. Albrecht and Creighton proposed a theory based on the charge transfer effect of the adsorbed molecule on the enhancement efficiency [49, 50]. This chemical enhancement theory relies on the charge transfer complex formation of the adsorbed molecule. However, it is difficult to separate these two effects experimentally. In the mid-1990s, an important development in electrochemical SERS (EC-SERS) was carried out by which substantial surface Raman enhancement could be imparted to the VIIIB transition metals of importance for electrochemistry and catalysis. Tian and his group at Xiamen University, China, developed several surface roughening procedures and demonstrated that the SERS effect can be directly generated on transition metals such as pure Pt, Ru, Rh, Pd, Fe, Co and Ni electrodes, and their surface enhancement ranges in general from one to three orders of magnitude. Since the early 2000s, the approach of replacing randomly roughened surfaces with well-controlled nanostructures of both coinages (eg. Au, Ag and Cu) and transition metals has been introduced as a promising class of highly SERS-active substrate [51]. Up to now, molecular level studies using Raman spectroscopy on diverse adsorbates at various material electrodes have been realized. These advances have made Raman spectroscopy a popular tool in electrochemistry. Moreover, a systematic study on EC-SERS processes could help elucidate comprehensively the SERS mechanisms.

1.11.2 Key Features of Surface Enhanced Raman Scattering

The pioneers summarized the key features of SERS as listed briefly below [52-54].

- It is a highly surface-sensitive, non-destructive and *in situ* vibrational spectroscopic technique.
- SERS has been observed at solid/liquid, solid/gas and solid/solid interfaces as an interface-sensitive technique. Molecules adsorbed in the first layer on the surface show the largest enhancement. However, the enhancement also has some long-range aspect with molecules separated from the surface by tens of nanometres showing some enhancement depending on the substrate morphology and physical environment.
- The excitation profile (scattering intensity versus excitation frequency) deviates from the fourth power dependence of normal Raman scattering (nRs).

- It has extremely high spatial resolution. The enhancement range is several nanometres, effective for one or several molecular layers close to the SERS active substrate.

- A very large number of molecules adsorbed on or near the surfaces of metals exhibit SERS, but their electromagnetic values could be very different. It depends on the bond type between metal and molecules.

The recent advancement in the field of SERS research is mainly focused in the following directions:

- Fabrication of new, novel and efficient SERS-active substrates to overcome the substrate generality of SERS.

- Single-molecule SERS to improve the molecule generality and enhance the detection limit of various adsorbates/species.

- Understanding the mechanisms involved in the SERS phenomenon.

- Use of SERS for imaging, sensing, diagnostics and further search for new applications.

1.11.3 Enhancement mechanisms in SERS

A number of SERS mechanisms have been proposed to explain the above-mentioned SERS characteristics. However, no one mechanism can explain all observed phenomena. Electromagnetic enhancement (EM) and chemical enhancement (CM) are two widely accepted mechanisms contributing to the SERS effect in recent years.

Generally, it has been widely accepted that the SERS enhancement effect is contributed by the long-range electromagnetic field enhancement (EM) and short-range chemical enhancement (CM). The former is the main contributor to SERS signals in most SERS systems. However, in case of electrochemical systems, CM also plays an important role, especially in characterization of chemical species as it is closely associated with the chemical property of surface species and substrates.

The EM mechanism is based on the amplification of the electromagnetic field generated due to coupling of the radiation field with the localized surface plasmon

(LSP) of the metal nanoparticles. The localized surface plasmon resonance (LSPR) occurs when a resonance condition between the incident wavelength of light and the electrons in the nanoparticles is achieved. This causes a collective oscillation of the conduction electrons and has two primary consequences. First, the wavelengths of light that cause this collective oscillation are selectively absorbed by the nanoparticles and can be monitored using UV–vis spectroscopy. The second is the formation of enhanced electromagnetic fields that extend from the nanoparticles surfaces. These fields are responsible for a large portion of the enhancement observed in SERS. The enhancement is roughly proportional to $|E^4|$ and generally in the order of 10^8 or more, where E is the intensity of the electromagnetic field.

Another important and common feature of EC-SERS is that the SERS intensity strongly depends on the electrode potential. The change in the electrode potential may result in a change in the coverage and/or adsorption orientation of the molecule, both of which will lead to a change in the SERS intensity.

1.11.4 Electromagnetic enhancement (EM)

a) Isolated metal sphere

This model consists of a single metal sphere, small compared to the wavelength of light, which is irradiated by a laser field. Raman scattering arises from molecules that are adsorbed on the surface of this sphere on ignoring the molecules in determining the field near the surface and assuming that the sphere is embedded in a medium (which could be vacuum or solvent) of dielectric constant ε_o. The dielectric constant is independent of the size of the sphere and inside the metal sphere is denoted by ε_i.

The electric field of the incident electromagnetic wave is $\mathbf{E}_o$, a vector that points along the z-axis, and that can be assumed independent of coordinates for distances at least as large as the sphere. Under these conditions, Maxwell's equations may be approximated by Laplace's equations to determine the field both inside and outside the sphere. The resulting field outside the sphere, $\mathbf{E}_{out}$, can then

be written as:

$$\mathbf{E}_{out}=E_o\,\mathbf{z}-\alpha E_o\left[\frac{\mathbf{z}}{r^3}-\frac{3z}{r^5}\left(z\mathbf{z}+x\mathbf{x}+y\mathbf{y}\right)\right] \qquad (1)$$

where the first term is the applied field, and the second is the induced dipole that results from polarization of the sphere electron density ρ is the metal polarizability, x, y, z, r, **x**, **y**, **z** are the usual Cartesian coordinates, radial distance and Cartesian unit vectors, respectively and E_o is the magnitude of $\mathbf{E}_o$. For a metal sphere with the dielectric constants indicated above, the polarizability is

$$\alpha = ga^3 \qquad (2)$$

where a is the sphere radius and

$$g=\frac{\varepsilon_i-\varepsilon_o}{\varepsilon_i+2\varepsilon_o} \qquad (3)$$

Note that the polarizability is a number that is on the order of the sphere volume in the limit of zero frequency, as in that case ε_i is $-\infty$. However, whenever the real part of ε_i equals $-2\varepsilon_o$ and the imaginary part is small, becomes very large, and as a result the induced field becomes large. It is this induced field that is responsible for the electromagnetic enhancement. This plasmon resonance condition requires the real part of ε_i to be large in magnitude and negative, and this is always the case for a free electron metal at long enough wavelengths. In addition, the formula says that the plasmon resonance wavelength will change when the dielectric constant ε_o of the external medium is varied. Indeed, since the metal dielectric constant typically increases (becomes less negative) as wavelength decreases, the resonance condition will be satisfied for longer wavelengths, i.e. red-shifts, as solvent dielectric constant increases.

The Raman intensity depends on the absolute square of $\mathbf{E}_{out}$ which we denote as E^2_{out}, evaluated at the surface of the sphere (i.e. r=a). From equation (1), this is given by

$$E^2_{out}=E^2_o\left[\left|1-g\right|^2+3\cos^2\theta\ (2\ \mathrm{Re}(g)+\left|g\right|^2)\right] \qquad (4)$$

where θ is the angle between the applied field direction and the vector r locates positions on the sphere surface. If $|g|$ is large, equation (4) reduces to $E E_{out}^2 = E_0^2 |g|^2$ (1+3 $\cos^2\theta$). This indicates that the largest field intensities are obtained for angles θ equal to 0° or 180°, i.e. along the polarization direction. Also, the ratio of the largest to smallest field enhancement as a function of θ is 4, and the angle integrated expression is 1/2 the peak intensity.

In Raman scattering the applied field induces an oscillating dipole in the adsorbed molecule. This dipole then radiates, and the component of this radiation that has been shifted by the vibrational frequencies of the molecule determines the Raman scattering intensity. In SERS the field in equation (4) determines the magnitude of the induced dipole, but there is also the possibility of enhanced emission from this dipole. This enhancement is more difficult to evaluate, as unlike the applied field E_o which is accurately described as being constant over the volume of the sphere, the emitted field is more complex. The proper treatment of this field has been given by Kerker *et al*. [55], to a first approximation that is appropriate for small particles [56], the enhancement is determined by an expression similar to equation (4), but evaluated at the Raman-shifted frequency. If we consider molecules located at the position of maximum enhancement and consider only the limit $|g|>>1$, then the overall enhancement arising from incident and scattered fields is approximately

$$\xi_R = \frac{E_{out}^2 E_{out}^{'2}}{E_o^4} = 16|g|^2|g'|^2 \qquad (5)$$

where the primed symbols refer to fields evaluated at the scattered frequency. The corresponding angle averaged enhancement factor would be smaller than this by a factor of 4. Equation (5) is identical to one derived by Kerker *et al* [55] using more rigorous theory. For small Stokes shifts, $|g|$ and $|g'|$ maximize at approximately the same wavelength, in which case if $|g|$ and $|g'|$ are both approximately 10 in magnitude, then the enhancement will be approximately 10^5. If we use the free-electron Drude model for the metal dielectric constant:

$$\varepsilon_i = 1 - \frac{\omega_p^2}{\omega(\omega + i\gamma)} \qquad (6)$$

where ω_p is the plasmon frequency and γ is the plasmon width, then the peak magnitude of g will be roughly 10. There are several materials such as Ag with the peak $|g|$>> 10. However the free electron model for the dielectric constant is rarely sufficiently accurate for this prediction to be quantitative. In fact, electromagnetic enhancements are generally rather small for spherical particles because the surface plasmons for most materials are far enough to the blue that γ is large (typically due to inter band transitions). Larger enhancements arise for prolate spheroidal objects, as the plasmon resonances for such objects occur at frequencies that are red-shifted relative to spherical particles to frequencies where the plasmon width is sufficiently small to make $|g|$ 10 or larger. For this reason we turn our attention in the next section to the electrodynamics of spheroidal particles.

The results obtained to this point are related closely to the extinction and scattering cross-sections for spherical particles, as obtained from the long wavelength limit ($a/\lambda << 1$) of Mie theory [54]. In particular, if we define $x = 2\pi a (\varepsilon_0)^{1/2}/\lambda$, then the extinction cross-section Q_{ext} is:

$$Q_{ext} = 4x \, \mathrm{Im}\,(g) \qquad (7a)$$

and the scattering cross-section Q_{sca} is:

$$Q_{sca} = \frac{8}{3} x^4 |g|^2 \qquad (7b)$$

where g is still given by equation (3). Evidently, if we leave out the x^4 prefatory (which varies as λ^{-4}), the wavelength dependence of equation (7b) is the same as the large $|g|$ limit of equation (4). In addition, as long as the Plasmon width is much smaller than the plasmon energy, the extinction cross-section has the same wavelength dependence (after leaving out the x factor) as the large $|g|$ limit of equation (4). Since the extinction cross-section is much larger than the scattering cross-section for a small metal particle, it has extinction that is most often compared to SERS excitation profiles. What we see therefore is that in the small particle limit, SERS excitation and extinction plasmon peaks and widths should be the same.

b) Electrostatics of isolated spheroids

The exact analytical solution to the electrodynamics of spheroidal particles is very complex, so the work done has involved either numerical solution of Maxwell's equations analytical electrostatic solutions [55-57] that are valid only for small particles. Although the numerical solutions are more accurate, the electrostatic solutions are more instructive. Fortunately, for particle sizes of significant interest to the experiments (<100nm), both theories give very similar results.

If we consider a spheroid whose major axis is of length 2*b* and minor axis 2*a*, with a constant field E_o applied along the major axis, then an explicit expression for the Raman enhancement factor for molecules that are randomly distributed on the spheroid surface (i.e. averaged over the surface) has been given by Zeeman and Schatz [58] as follows:

$$\xi_R = R(\omega)R(\omega-\Delta) \tag{8}$$

where

$$R(\omega) = |1-g|^2 + \left[\frac{2\,\mathrm{Re}(1-g)g^*}{Q_1(\xi_o)} + \frac{|g|^2}{Q_1^2(\xi_o)(\xi_o^2-1)}\right] \times \left[\frac{-\left|(\xi_o^2-1)^{1/2} + \xi_o^2 \sin^{-1}(1/\xi_0)\right|}{(\xi_o^2-1)^{1/2} + \xi_o^2 \sin^{-1}(1/\xi_o)}\right] \tag{9}$$

$$\xi_o = \left(1-\frac{a^2}{b^2}\right)^{-1/2} \tag{10}$$

$$Q_1(\xi_o) = \frac{1}{2}\xi_o In\left(\frac{\xi_o+1}{\xi_o-1}\right) - 1 \tag{11}$$

and

$$g = \frac{\varepsilon_i - \varepsilon_o}{\varepsilon_i + \chi\varepsilon_o} \tag{12}$$

The parameter χ in equation (12) is given by

$$\chi = -1 + \frac{1}{(\xi_0^2 - 1)\left[\frac{\xi_o}{2} In\left(\frac{\xi_o + 1}{\xi_0 - 1}\right) - 1\right]} \qquad (13)$$

Note that g in equation (12) is a generalization of that in equation (3). In fact the parameter χ=2 for a sphere, but for prolate spheroids, i.e. those with b > a(ξ_o-1) > 1, χ is larger than 2 and for oblate spheroids (ξ_o < 1) it is less than 2. When c is greater than 2, the plasmon resonance condition, Re (ε_i + $\chi\varepsilon_o$)=0, is satisfied for a wavelength that is to the red of that for a sphere (due to the fact that for metals, the real part of ei is, according to equation (7), more negative for longer wavelengths). Ofcourse this also means that for oblate spheroids, the resonance will be blue shifted relative to a sphere. However, it should be noted that the resonance described here refers to an incident field with the electric polarization parallel to the symmetry axis of the spheroid. There is another plasmon resonance associated with excitation perpendicular to the symmetry axis. This resonance is identical in frequency to the parallel resonance for a sphere, but it shifts in the opposite direction for a spheroid, i.e. blue-shifting for prolate spheroids and redshirting for oblate spheroids. Indeed, the expression for g in equation (12) still applies, but the expression for χ is:

$$\chi = -1 - \frac{1}{\frac{1}{2}\xi_o\left(\xi_o^2 - 1\right) In\left(\frac{\xi_o + 1}{\xi_0 - 1}\right) - \xi_o^2} \qquad (14)$$

Thus we see that both oblate and prolate spheroids have plasmons that are red-shifted relative to the sphere case. Since most SERS-active metals (Ag, Au, and Cu) exhibit free electron-like behaviour at long wavelengths, it is the red-shifted plasmon resonance that contributes most to SERS. Thus, non spherical particles, either prolate or oblate, give larger SERS intensities than spheres. In addition, we see that increasing the dielectric constant of the external medium, e_o leads to additional red-shifting of the Plasmon resonances, just as with the sphere case that we described earlier. Equation (9) refers to the enhancement averaged over the surface of the spheroid. In some applications it is also of interest to have an expression for the enhancement as a function of location on the surface. This expression is given by:

$$R(\omega,\eta) = |1-g|^2 + \left[\frac{2\,\mathrm{Re}[(1-g)g^*]\eta^2}{Q_1(\xi_o)(\xi_o^2-\eta^2)} + \frac{|g|^2\eta^2}{Q_1^2(\xi_o)(\xi_o^2-1)(\xi_o^2-\eta^2)} \right] \quad (15)$$

Note that this expression depends on the spheroidal coordinate η, which is related to the usual spherical polar coordinate θ via:

$$\eta = \cos\theta \sqrt{\frac{\xi_o^2 - 1}{\xi_o^2 - \cos^2\theta}} \quad (16)$$

Hence the electromagnetic theory for SERS molecules adsorbed on spherical metal particles predicts that a strong enhancement will be observed with the following conditions a 1) the particle size must be smaller than wavelength, 2) the frequency of excitation must be near the surface Plasmon resonance condition and 3) the molecule cannot be too for the surface.

1.11.5 Chemical enhancement (CE)

A further contribution of the enhancement of the Raman signal is given by mechanisms of chemical nature. The molecule must be directly adsorbed to the roughened surface in order to experience the chemical mechanism. Chemical enhancement accounts for 10-100 (relatively small, but nevertheless important) of the total enhancement factor and requires the molecule to be in direct contact (bonded) with the surface of the metallic nanostructure [59]. When there is an electronic coupling between the molecule and the metal, the Raman cross-section of the molecule increases due to the charge transfer from the metal to molecule. A charge transfer between the molecule and the metal leads to the broadening and shifting of the electronic level in the adsorbed molecule resulting in a ‘resonance’ Raman effect which gives SERS enhancement. A dynamic charge transfer takes place when a photon is absorbed by a metal which result in a hot electron state. Two types of charge transfer mechanisms could be envisioned, ie, molecule to metal and metal to molecule charge transfer. In molecule to metal charge transfer, an electron is transferred from the Highest Occupied Molecular Orbital (HOMO) to the Fermi level of the metal. In metal to molecule charge transfer an electron is transferred from the Fermi level of the metal to the Lowest Unoccupied Molecular Orbital (LUMO). The hot electron gets transferred to the LUMO of the molecule. The increase in the

LUMO electron leads to increased Raman signal due to increased probability of electron-photon coupling in the Raman scattering tensor. The excited electron is later transferred back to the metal from the LUMO and this result in the emission of stokes photons. This mechanism is called the first layer effect. The direct attachment of the molecule to the surface gives a higher enhancement factor [60]. Chemical enhancement can be explained by a resonance-like Raman mechanism. Figure 1.3 depicts the operative charge transfer mechanism for a molecule adsorbed on an electrode. The resonance Raman process is highly unlikely because of the large energy gap between the HOMO and the LUMO in spite of the disturbed relocation of the energy level for a molecule adsorbed on a rough surface. However, the resonance Raman scattering can occur through photon-driven charge-transfer processes between the metal and adsorbates. It is assumed that transitions from states near the Femi level are preferred because of favourable matrix elements involving wave function overlap of localized electron density of states. The whole process can be identified by the following four steps [61]

Step 1: An electron-hole pair of the metal is created by the incident photon with energy $h\nu$, and the electron is excited as a "hot electron";

Step 2: The so-called "hot electron" tunnels into the accessible vacant levels, such as the LUMO of the adsorbate, generating a charge-transfer excited state;

Step 3: A negative ion (adsorbate molecule-electron) created in step 2 has an equilibrium geometry differing from that of the original adsorbate molecule and the electron will return to the metal and the nuclear in the adsorbate will get relaxed during this charge-transfer process;

Step 4: The electron will recombine with the hole created in step 1, which leads to a vibrational excited neutral molecule and to emission of a Raman-shifted photon with energy $h\nu$.

In general, chemical effects contribute to SERS in a short range, on the molecular scale. This mechanism depends on the adsorption site, the geometry of bonding and the energy levels of the adsorbate molecules. Although the CE mechanism is not a general mechanism and is restricted by its chemical specificity, it

can provide useful information uniquely on chemisorptive interactions between metals and adsorbates.

Considering the Herzberg-Teller contribution to the charge transfer theory, J.R. Lambari [61] suggests that in molecule to metal charge transfer system (Figure 1.4) charge transfer takes place from the molecular ground state to one of the unfilled metal levels. This transition gains its intensity via $M_{MI,}$ through intensity borrowing from the allowed transition I-K. The borrowing mechanism is vibronic coupling through h_{MK}, which represents coupling of the metal to the excited molecular states through some vibrational mode. In metal to molecular charge transfer system, charge transfer takes place from one of the filled metal level M to the excited state K. This transition obtains its intensity via M_{MK}. (M-metal level; I,K-ground and excited state of molecule; M_{IK}, M_{MK}-Matrix elements representing molecule to metal and metal to molecule charge transfer transitions).

The Raman intensities of the adsorbed molecules are resonantly enhanced when the incident photon energy (hν) matches the energy difference between the charge transfer state of the molecule and the Fermi level of the metal, in the case of molecule charge transfer mechanism whereas, in the case of molecule transfer processes, a similar resonance condition should be fulfilled between the position of the Fermi level and the energy of the molecular ground state. So in the charge transfer enhancement of SERS intensity, the electronic level of both the adsorbed molecule and the metal are involved. Since the energy of the Fermi level depends on the applied potential, one can fulfil the enhancement condition by changing the energy of the applied potential. As a result the potential corresponding to the maximum of SERS intensity changes with hν. The direction of charge transfer is determined by the relation between the applied change in Fermi energy and the resulting shift in the transition energy. A red shift which results from raising the Fermi energy would mean that the charge transfer occurs from a filled metal orbital to an empty adsorbed orbital and an opposite trend will occur for blue shift [62, 63].

1.11.6 Characteristics of SERS

a) Surface enhancement factor

SERS technique provide greatly enhanced Raman signal from Raman active molecules that have been adsorbed on certain specially prepared metal surface.

The intensity of surface enhanced Raman signal has been regularly observed in the order of 10^4-10^6 and can be as high as 10^8 and 10^{14} for some system [64]. Silver, gold and copper show enhancement of the order of 10^6. Maximum values of electromagnetic enhancement for isolated single colloidal silver and gold spheroids are in the order of 10^6 to 10^7. This factor ranges from one to four orders of magnitude for transition metals. Metals such as Pd or Pt exhibit enhancement of about 10^2-10^3 for excitation in the near UV [64]. For silver nanoparticles excited with visible laser wavelength show the intrinsic enhancement factors as high as10^{14}-10^{15} [65].

b) Temperature effect

The relative intensities of the SERS bands change dramatically with temperature, which indicates the transformation of the tauterizms or the reorientation of the molecules on the surface layer [66].

c) pH dependence

` Variation in the SER spectra with changes in pH were usually attributed either to a change in orientation of adsorbates with respect to metal surface or to a change in chemical nature of the adsorbates [67].

d) Depolarization ratio

The laser light is polarized parallel to the scattering plane i.e. polarized. In this case, the depolarization ratio is defined as the ratio of $I_{||}/I_{\perp}$, where $I_{||}$ and $I_{\perp}$ are the intensities of scattered radiation polarized parallel and perpendicular to the scattering plane.

The depolarization phenomenon of the Raman scattering offers the evidence to distinguish between the SERS and the normal Raman spectrum (nRs) for the solution phase. For the nRs of molecules in the solution phase, the depolarization ratio of non-totally symmetric modes is closed to 0.75, but for highly symmetric modes it is close to zero. However in a SERS spectrum of both symmetric and non-symmetric modes for adsorbed molecules have similar depolarization values (0.6-0.75) [61].

The increase of depolarization ratio in non-resonant SERS experiments of small molecules such as pyridine might be related to the lowering of the vibrational symmetry of the molecule geometry, as modified by adsorption to the metal and also due to lower field gradients. The depolarization ratio is larger in surface enhanced resonance Raman scattering (SERRS) compared to RRS. This is attributed to a lowering of symmetry arising from the very large field gradients on the metal colloidal clusters [68].]. The depolarization is easily explained by considering a SERS active surface to be a heterogeneous collection of roughness features of different size and shapes onto which the molecules adsorb in a variety of orientations. Both lack of motional averaging and the opportunity of multiple scattering contribute to depolarization [59].

e) Solvent effect

In general, large the hydrogen bonding capability of the solvent and smaller the solvent molecular size, the speed of the replacement kinetics will be grater. Thus solvent desorption and subsequent SERS activity for most adsorbates occur faster in water followed by methanol, N, N-dimethylformamide and acetonitrile. However, the adsorbate having large aromatic ring system or nitrogen containing heterocyales tend to cause a faster solvent desorption [69].

(f) Metal Substrate

SERS spectra are obtained on a number of metal substrates such as Ag, Au, Cu, Pd, Pt, Li, Na, K, Al, In, Ni, Co, Rh, Ru, Ga and Fe etc [65]. The dominance of the coinage metals and the alkali metals as SERS substrates arise simply because the resonance condition is satisfied at the visible frequency commonly used for Raman spectroscopy. Other metals have their surface Plasmon resonance in different region of electromagnetic spectrum [70].

(g) Excitation profiles

The excitation profile (scattered intensity vs. exciting frequency) deviates from the fourth power dependence of normal scattering [53]. Desorption or electrode reactions affect the shape of the intensity profile [61]. The broad resonance observed may be due to the characteristic of the substrate, the adsorbate or the combined

system. It's depended upon electrode potential in electrochemical experiments and may be different for different vibrational modes. The spectral profile is a sensitive measure of the distribution of surface sites, which affects the Raman enhancement. In indicates a slight asymmetry in this surface distribution and also depends on the metal substrate. The excitation profile maximum on silver was located in a shorter wavelength region than on Cu or Au. The excitation profile maximum varies depending upon the nature of the metal interface for a given metal- substrate system.

h) Line shape

The spectral lines associated with molecular vibrational frequency are broadened on adsorption. This occur as a result of 1) a distribution of molecular surface distance, 2) a distribution of angles of the molecular planes with respect to the surface, 3) a distribution of detailed surface sites reflecting surface roughness and 4) the nature of the intermediate state in SERS.

i) Range dependence

Jensen et al. found that the enhancement factor changes for particles of varying hights, even when the diameter of the particle was kept constant. The enhancement factor $G= ((r/(r+d))^{1/2}$ for single molecule at a distance d from the surface of a sphere of radius r or $G=((r/(r+d))^{10}$ for a monolayer of molecules [71].

j) Surface roughness

The frequency of the incident light is effective in producing the intense electromagnetic field on the particle and it is depend on the characteristics of the roughness features as well as on the type of the metal used.

The roughness features are of the order of tens of nm; small compare to the wavelength of the incident excitation radiation. These roughness features can be developed in a number of way; for example oxidation-reduction cycle (ORC) on electrode surface, vapor deposition of metal particles on the substrate, metal spheroid assemblies produced via lithography, metal colloids and metal deposition over a deposition makes of polystyrene nanospheres [72].

k)Observation of forbidden mode

The observation of silent modes inn Raman is reported based either on the existence of an electric gradient in the interface or on the lack of symmetry caused by the formation of the surface complex [73].

1.11.7. Selection rules

The surface selection rules is an important part of SERS theory, which determines the activities or silence of normal modes and whether the intensity of the normal mode is enhanced or not in the Raman scattering process.

There are two popular ways of stating the surface selection rule for the SERS. One is to invoke in terms of the image field model [74, 75] and another one is based on the enhancement of the local electromagnetic fields for the flat and spherical metal surface [76].

1.11.7.1 Image field model

In this model, a dipole located near the surface induces an image dipole within the metal [77]. A dipole parallel to the metal surface as an image dipole in the opposite direction while the image a dipole perpendicular to the surface is in the same direction as that of its shows, which results in screening of parallel dipoles and reinforcement of perpendicular dipoles. Therefore the adsorbate-metal system can be recorded as molecular dipole-image dipole system.

The surface selection rule for Raman scattering in terms of image changes was reported by hexter et al. [75]. He proposed that the process of finding the image of each dipole is equivalent to the addition of a new symmetry operation that characterizes the new system involving the adsorbed molecule and the metal. He conclude that modes belonging to irreducible representation spanning the x^2, y^2, z^2,xy and yx components of the derived polarizability will be active while dose transforming as xz and yz will be extinguished on the surface [75], where z axis is selected to be normal to the surface and x and y axis lie in –plane. By considering the image dipole criterion simultaneously, and insisting on normal electric field at the surface, Richardson and sass conclude that only vibration, which transform like the z^2 polarization components, are being surface active [78].

From this point of view, in the image model, the surface effect is replaced by the image dipole/charges, while the surface detail is neglected in the surface selection rule. The surface rule become progressively more valid in spectral regions for which the metal is a good reflected, for intense, in the IR and its less valid in the visible or near UV region of the spectrum in which many transition metals are not good reflectors [79].

1.11.7.2. Electromagnetic field model

In this model, the surface selection rules arises from the fact that the incident and reflected electric fields are directed at the surface interface in such a way that the tangential component is diminished while the normal component is augmented consequently, the components of transition dipole normal to the surface are excited more strongly than tangential components [80].

For the molecule on the flat surface, one must consider both the state of polarization of the incident ray and the scattered ray. Mokovits [81] suggests that for Raman there are three classes of vibrational modes with distinct spectral behavior: 1) those exited only by the normal components on the field and resulting is an induced dipole with a strong component only in the direction perpendicular of the surface, 2) those existed only by the tangential components of the field and resulting in an induced dipole with a strong component tangential to the surface and 3) the mixed case. If z be the surface normal, vibrational mode possessing polarizability components α_{zz} belongs to the first type(most intense spectral feature), irreducible representation α_{xx}, α_{yy} and α_{xy} belongs to the second types (decrease in the intensity) and α_{xz} and α_{yz} belongs to the third type (very weak and commonly absent), where α is the polarizability tensor.

For spherical colloidal metal surface, the square of the radial and tangential field components are given by

$$\overline{E_t^2}\ \alpha 2E_0^2\left|1-g\right|^2; \qquad \overline{E_n^2}\ \alpha E_0^2\left|1+2g\right|^2 \tag{17}$$

Where E_0 is the incident field strength and

$$g=\frac{\varepsilon-\varepsilon_o}{\varepsilon+2\varepsilon_o} \tag{18}$$

The electromagnetic SERS enhancement is the product of the field intensity associated with the incident and scattered beams. Hence the three classes of vibrational modes are expected to have the following SERS enhancement.

$$\alpha_{zz} : \left(\overline{E_n^2}\right)\left(\overline{E_n'^2}\right)\alpha\left|1+2g\right|^2\left|1+2g'\right|^2$$

$$\alpha_{xz},\ \alpha_{yz} : 1/2\left[\overline{E_n^2 E_t'^2} + \overline{E_t^2 E_n'^2}\right]\alpha\left[\left|1+2g\right|^2\left|1-g'\right|^2 + \left|1-g\right|^2\left|1+2g'\right|^2\right]$$

$$\alpha_{xx},\ \alpha_{yy} \text{ and } \alpha_{xy} : \overline{E_t^2 E_t'^2}\alpha 4\left|1-g\right|^2\left|1-g'\right|^2 \qquad (19)$$

where the prime indicates the properties calculated at the Raman shifted frequency, while unprimed quantities are calculated at incident frequency.

The SERS excitation profiles associated with the three types of modes may be predicted from the wavelength dependence of the quantities on the right hand side of equation (3) to the red of the surface-plasmon frequency, α_{zz} modes show that enhanced spectral features relative to the others. To the blue of the surface-plasmon frequency, the $\overline{E_n^2}$ progressively decreases in comparison with $\overline{E_t^2}$ causing diminishing in intensities of α_{zz} modes [82].

1.12 SERS substrate

When SERS was imaginary, it twisted out that only a few ‘free-electron-like’ metals, mainly Ag, Au and Cu could provide a large SERS effect for roughened metal surfaces and metal particles with dimensions in the order of nanometres. As the SERS activity strongly depends on the nature of the substrates to be used for SERS effect, lack of suitable SERS substrates other than those mentioned above gave rise to lack of ‘substrate generality’ of SERS in the early 1990s. This means transition metals such as Ni, Pd, Pt, Co cannot be used as SERS substrates. Therefore, it is important to microscopically understand the origin of SERS from metal, especially metal nanoparticles. In general, electromagnetic field enhancement mechanisms contributes to a large part in the overall enhancement observed in SERS effect, which can be determined by the interaction of light (incident and scattered) and metal. It generates SPR at metal nanoparticles or surface nanostructures used as substrates. The electromagnetic field of the light at the surface can be greatly enhanced under conditions of SPR for ‘free-electron’ metals such as Au, Ag and Cu. The conduction

electrons in these metal nanoparticles can be driven effectively by visible light to cause collective oscillation of these electrons, generating a strong electromagnetic field near the surface of metal nanoparticles. To meet the conditions of good SPR, the metal usually should have a low value of the imaginary component of the dielectric constant. This is impossible for a transition metal because in the visible light region the values of the imaginary part of the dielectric constant is large and inter band excitation occurs as the Fermi level is located at the d-band. In addition, there is coupling between conduction electrons and inter band electronic transitions. This can depress considerably the quality of the SPR of transition metals. Accordingly, the SERS activity of electrochemically roughened transition metal surface is in general quite low, with typical surface enhancement factor ranging from 10 to 10^3.

The word 'molecule generality' means getting good SERS signal and to improve the detection sensitivity of SERS technique with a large variety of molecules. Therefore, it is challenging to obtain high-quality SERS spectra even from a single molecule adsorbed on SERS substrates. The overall improvement of SERS signal with an enhancement factor up to 10^{14} can give rise to high quality single-molecule SERS spectra and can improve the detection sensitivity up to single-molecule level. The achievement of single molecular sensitivity of the SERS technique can improve the 'molecular generality'.

The development of nanoscience and nanotechnology boosted the scientific community and attracted a wide interest in SERS again in the 2000s. Thus, SERS has become an important branch of nanoscience and nanotechnology. It has been found that SERS activity depends on the size, shape and aggregation of nanoparticles. Several techniques of nanoscience have been employed to fabricate and characterize SERS related nanoparticles or nanostructures in a well controlled fashion. Such efforts have led to the significant progress in this versatile field. High-quality SERS spectra from a single molecule adsorbed on well-characterized Au and Ag nanoparticles have been obtained with a high signal enhancement up to 10^{14}. The high-quality single molecular SERS spectra a promising tool for trace analysis in life and medical sciences as well as security and environment protection.

1.12.1 SERS Substrate: an overview

SERS-active substrate fabrication is an important field in SERS research. The two most common SERS-active substrates are metal colloids of coinage metals like Au, Ag and Cu obtained from chemical reduction and the metal electrode surfaces roughened by one or more electrochemical oxidation–reduction cycles. The recent advancement of nanotechnology has been utilized to fabricate various nanostructures from nanoparticles to nanorod, nanosphere, nanowires, which can be used as SERS-active substrates. The SERS substrates can be roughly classified into three categories: (1) metal nanoparticles in suspension, (2) metal nanoparticles immobilized on solid substrates and (3) nanostructures fabricated directly on solid substrates, which includes nanolithography and template-based synthesis of nanostructures. Although nanoparticles and nanoparticles film electrodes show good surface uniformity, it is difficult to control the spacing of the nanoparticles to optimize the SERS activity. Templates methods can provide highly ordered SERS substrates with controlled inter particle spacing. The various method of SERS-active surfaces available today, e.g., colloids, solid, colloid in sol-gel [78], electrochemically roughened electrodes, vapour-deposited metal island films [79], solution of combustion and lithography-produced nanostructures [80] are being most widely used for the fabrication of SERS-active substrates.

However, the distribution of shapes and sizes and the ease of aggregation will influence the surface-enhancing properties. Among the metal surfaces used as SERS active substrate with appropriate roughness, silver nanoparticles have shown suitable physical properties for an optical electromagnetic field enhancement due to the fractal morphology that result upon their aggregation [81].

a) Silver colloid

Two main methods have been employed so far to obtain silver colloids with good properties to be employed as SERS substrate involving the chemical reduction of silver nitrate with sodium borohydride and with sodium citrate.

Silver colloid was prepared by Dirk and Charles borohydride-reduced method [82]. In brief, silver nitrate ($AgNO_3$) solution and sodium borohydride ($NaBH_4$) solution were prepared by dissolving 0.0294mM of $AgNO_3$ in 100ml of distilled

water and 0.0096 mM of $NaBH_4$ in 300ml of distilled water. 100ml of $AgNO_3$ solution was added dropwise to 300 ml of ice-cold $NaBH_4$ solution and the mixture was stirred vigorously for 1 hour until glassy yellow colour was obtained. The prepared Ag colloidal solution has a single absorption maximum at 392nm consists of roughly spherical particles of diameter in the range 1-50nm. The silver colloid was stored in a dark place, which was stable for several days or weeks.

It was also prepared by following the citrate reduction procedure reported by Lee and Misel [83], 90mg of $AgNO_3$ was dissolved in 500ml distilled water and the solution was heated to 100°C. A 1% sodium citrate was added to 10ml of distilled water under vigorous stirring and the solution was boiled for 60mins with continuous stirring. The resultant silver solution shows maximum absorption at 420nm.

b) Gold colloid

A gold solution was prepared by reduction of $2.5x10^{-3}$M chloroauric acid ($AuCl_4$) 1ml with $1x10^{-3}$M $NaBH_4$ solution (3ml). The solution was purple in color and showed maximum extinction at 525nm, characteristic of gold particles smaller than wavelength [84].

c) Copper colloid

Copper colloidal nanoparticles have been prepared by adding 5mL of cupric nitrate 10^{-2}M solution to 60ml of sodium citrate (5.6×10^{-3} M). In order to avoid the oxidation of copper colloids, 30ml of $NaBH_4$ and sodium hydroxide (NaOH) solution (2×10^{-2}M) was added drop wise. The resulting colloid is a yellow-brown color and changed to dark red after 1hr. The colloidal became dark red showing absorption maximum at 560nm. Colloid silver and gold hydrosols also appear to provide efficient media for SERS measurements. An attribute of the technique using metal colloids is, unlike nanostructures on solid substrates, the sizes of the hydrosols are not uniform from batch to batch. Selection of colloidal particles with optimal sizes requires a tedious procedure [85]. Colloidal stability has been a major problem. Another disadvantage of colloid hydrosols is their tendency to aggregate in solutions and to flocculate at the bottom of the sample holders. Colloidal solutions tend to coagulate making them not very stable and difficult to use.

d) Metal electrodes

Electrochemical cells using silver electrodes and other metal electrodes have been used for SERS studies [86]. Silver at the electrode is oxidized by the reaction $Ag \rightarrow Ag^{+} + e^{-}$ during the first half of the cycle. During the reduction half cycle, a roughened silver surface is reproduced by the reaction $Ag^{+} + e^{-} \rightarrow Ag$. This oxidation-reduction procedure generally produces surface protrusions in the size range of 25-500nm on the electrode surface. The working electrode is generally placed in a position such that the laser excitation can be focused onto its surface and the Raman scattered light can be efficiently collected by appropriate optics. Strong SERS signals appear only after an electrochemical oxidation-reduction cycle, often referred to as `activation cycle', is performed on the metal electrode. Other metal electrodes such as platinum [87, 88] have also been investigated as SERS substrates. Experimental factors such as the influence of laser illumination of copper electrodes during oxidation / reduction treatment on SERS signals of pyridine and benzotriazole have been investigated [89, 90]. Photo alterations of the copper electrode can result in a further 10-fold increase in SERS. Beer et al. [91, 92] have investigated the ex situ versus in situ electrode roughening procedures for SERS on gold and silver electrode surfaces.

e) Metal nanoparticles island films

The simplest metallic nanostructure can be produced by evaporating a thin layer (less than 10nm thickness) of a metal such as silver directly onto a solid base support. Under these conditions the silver layer forms nanoparticles on the support in the form of isolated metal islands. On increase of the deposited silver thickness, the particles would start to combine and form a continuous film. The size and shape of the metal nanoparticles can be influenced by varying the thickness of metal deposited (as measured by a quartz crystal monitor perpendicular to the evaporation source). The silver films had extinction maximum that ranged between 450-660nm. SERS measurements using silver nanoparticles island films were compared with those obtained with other nanostructure materials [93, 94]. SERS from copper and zinc phthalocyanine complexes from silver and indium island films have been reported [95, 96]. The silver and indium films were vacuum evaporated ($p<10^{-6}$ torr) onto tin oxide glass slides and then coated with copper and zinc phthalocyanine complexes in

a vacuum system at a base pressure of $5x10^{-7}$ torr. Metal thickness was about 7.5 nm on the substrates in order to produce metal nanoparticles islands. Van Duyne et al. [97] characterized the surface roughness and nanometer scale structure of Ag films using atomic force microscopy (AFM).

(f) Sol-Gel process

The sol-gel process is also a controlled precipitation process [98]. The formed particles of small sizes will not precipitation but rather disperse in the solution as stable colloidal particles can agglomerate with each other to form precipitates of particle networks (gel) [99]. Solubility variations with temperature can be used to prepare sol. First, the substance is added or dissolved or mixed into a solution slowly and the sol forms once the solubility limits is exceeded. Then, the mixed solution is placed within capped polystyrene tubes to form gel. The solvent is allowed to evaporate from the gel. During densification the sol-gels are shrinking. After the shrink samples completes the annealing, the nanopowder is formed. Further, the formed sols were aged for several days. The gel powder samples were further dried and annealed at elevated temperatures to calcinate hydroxides.

(g) Homogeneous precipitation

In a normal precipitation process, aqueous solutions of reactants are mixed to produce precipitates of insoluble substance by exceeding the solubility limits. Since the mixing processes are not controlled, large concentration gradients during mixing produce a broad distribution of particles sizes. The mixtures, with magnetic stirring are then heated to boil. Due to this process NH_3 molecules during thermal hydrolysis of urea, there was essentially no concentration gradient in the solution. The resulting precipitate was washed with water and acetone. It was found that urea played a critical role in the precipitation process. In sol-gel processes, precipitation condition, such as solution pH, temperature, reagent concentrations, stirring rate, addition rate and aging time, must be controlled precisely to achieve uniform nucleation throughout the solution. Most of these methods involve complicated steps, expensive chemicals and takes longer processing time.

h) Combustion method

Combustion method is one of the gas phase (aerosol) methods generally producing powders ready to use, which are largely investigated and widely employed in the large-scale production of several metal oxide semiconductors. Combustion synthesis has been used to prepare many simple and complex oxide ceramics, such as aluminates [100], ferrites [101] and chromites [102]. In combustion synthesis, an aqueous solution of an oxidizer, typically a mixture of metal nitrate of the metal elements in the target product and an organic fuel (like urea, glycine, hydrazides (carbohydrazide-HCH), oxalyldihydrazide (ODH), malonic acid dihydrazide (MDH), tetra formaltrisazine (TFTA), carbohydrazide (CH), N,N-diformylhydrazine (DFH) and citric acid etc.) is dehydrated and ignited in a muffle furnace or on a hot plate at a temperature less than 350°C. The dehydrated mixture undergoes a vigorous, exothermic oxidation-reduction reaction. The heat creates a flame for few minutes, resulting in voluminous and foamy powder product occupying the entire reaction container. The exothermic combustion reaction releases a large amount of heat, which can quickly heat up the system to reach a temperature higher than 1600°C [103]. The combustion method results in uniform and pure powders of high surface-to-volume ratio. The mechanism of nanoparticles formation in the combustion synthesis is not complicated. Many parameters have to be considered, including the type of fuel, the fuel-to-oxidizer ratio, the use of an assistant oxidizer, the ignition temperature and the water content. Among the other methods, combustion synthesis processing offers many advantages which include low processing temperature, high purity, molecular level homogeneity and more flexibility in the components.

1.13 Advantages of combustion method

Compared to other chemical methods, the main advantage of combustion synthesis is as followed:

- It is reproducible.
- Cost-effective and simple procedure.
- Simple equipments are needed.
- High yielding nanoparticles without aggregation.
- It may control the shape of the particles.
- Use less toxic precursors: in water.
- With as few synthetic steps as possible.
- It minimizes the quantities of generated by-products and waste.

1.14 A Review- Orientation of SERS

In the last decade, remarkable progress has been made in the field of orientation of SERS studies. It has its importance not only in physical science but also in chemical, biological and medical science. Recent years have seen an enormous popularity of using SERS methodology to study a variety of biomolecules. Recently, a number of important breakthroughs in this field have been made, notably for the development of new applications. In the field of spectroscopy, a number of papers on SERS have been published. More specifically, recent papers are focused on the orientation of bio molecule and organic molecule adsorbed on metal surface.

B. Wang et al. [104] has reported the orientation of vitamin B12 molecules adsorbed on variation of copper electrode potential from 0 to -1.0 V and was studied by surface-enhanced Raman spectroscopy (SERS). An excellent SERS substrate was obtained with insitu electrochemical oxidation-reduction cycle (ORC). Assignments of Raman peaks observed by normal Raman spectrum (nRs) and SERS spectra of vitamin B12 molecule were given based on previous literatures. It was found that the potential-dependent relative intensity changed in SERS spectra which depended on the vitamin B12 molecular orientation with respect to the copper surface according to the surface selection rule (SSR). It was concluded that the corrin ring was adsorbed in tilt form on copper surface and the Co-CN group was farther away from the copper surface at higher potentials. With the decrease in potential, the tilt angle between the corrin ring and copper surface became smaller, then the Co-N group and 5,6 dimethylbenzimidazole group got close to the copper surface. The results offered an important structural attribute of vitamin B12 molecule when it interacted with copper electrode for the first time, and supplied a meaningful reference for the electrochemical bioactivity of the vitamin B12 molecule.

M. Umadevi et al. [105] studied the interaction between 2,3-bis(chloromethyl)anthracene-1,4,9,10-tetraone (BCMAT) on copper nanoparticles (NPs) by SERS. Copper NPs have been prepared by the chemical reduction method. The observed ring stretching modes show higher downshifts, broader bandwidths, and higher enhancement. The observed features in out-of-plane and in-plane CH deformation modes indicate that the BCMAT molecules may be adsorbed in a “flat-on” orientation on the copper NPs. The observed lower enhancement factor of the in-

plane C=O deformation mode and C=O stretching mode and the higher enhancement factor of out-of-plane C=O deformation mode elucidate that the BCMAT molecules are adsorbed on the copper NPs in a "flat-on" orientation. All these observations show that BCMAT is adsorbed on copper NPs through the π-anthraquinone ring system in a "flat-on" orientation.

D. Sajan et al. [106] studied the surface enhanced Raman scattering Single crystals of (S)-phenylsuccinic acid (SPSA) on silver surface at room temperature by the slow evaporation technique. The vibrational wavenumber of the adsorption geometry of (S)-phenylsuccinic acid (SPSA) on a silver surface have been simulated using DFT-B3PW91 with LANL2DZ basis set and it compared with the experimental spectrum. The large enhancement of in-plane bending and ring breathing modes in the surface-enhanced Raman scattering spectrum indicates that the molecule is adsorbed on the silver surface in an 'at least vertical' or slightly tilted orientation, with the ring perpendicular to the silver surface. The calculated vibrational spectra are in agreement with experimental values confirming the validity of the proposed adsorption configurations.

I. B. Cozar et al. [107] investigated the paroxetine's structure by different vibrational spectroscopic methods (FTIR, Raman and SERS), as well as density functional theory (DFT) calculation on (IUPAC name: (3S,4R)-3- [1,3-benzodioxol-5-yloxy) methyl]-4-(4-fluprophenyl) piperidine. After the identification of the lowest energy conformer of the investigation molecule, the FTIR, FT-Raman and SERS spectra were assigned on the basis of DFT calculation at B3LYP/6-31G(d) level of theory. The very good correlation was found between experimental and theoretical data which is clear evidence for a reliable assignment of the vibratiional bands. The molecular electrostatic potential of preferred adsorption sites of the paroxetine molecule on the silver nanoparticles surface. Based on SERS spectra analysis it is shown that the molecule is adsorbed on the silver surface through the benzodioxol ring, in a tilted orientation.

Y. Sheena Mary et al. [108] analyzed and recorded the IR, Raman and Surface Enhanced Raman scattering (SERS) spectra of L-proline. The molecular plane assumes a titled orientation with respect to the metal surface. The vibration

wavenumber and corresponding vibratiional assignments are examined theoretically using the Gaussian 03 set of quantum chemistry codes.

P. L. Anto et al. [109] recorded and analyzed the FT-IR and FT-Raman spectra of anilinium suflate. The Surface Enhanced Raman Scattering (SERS) was recorded from silver electrode. The vibratiional wavenumber of the compound have been computed using the Hartree-Fock/6-31G* basis and compared with the experimental values. The molecule is adsorbed on the silver surface with the benzene ring in a tilted orientation. The presence of amino and sulfate group vibration in the SERS spectrum reveal the interaction between amino and sulfate groups with silver surface. The direction of the charge transfer contribution to SERS has been discussed from the frontier orbital theory.

H. Tresa Varghese et al. [110] recorded and analyzed the IR and Raman spectra of disodium terephthalate. Surface Enhanced Raman Scattering (SERS) spectrum was recorded in silver colloid. The vibratiional wavenumber of the compound have been computed using the Hartree-Fock/6-31G* basis and compared with the experimental values. SERS studies suggest a flat orientation of the molecule at the metal surface.

Y. Sheena Mary et al. [111] recorded and analyzed FT-IR and FT-Raman spectra of 2-(β-fluorobenzyl)-6-nitrobenzoxazole. A surface enhanced Raman scattering spectrum (SERS) was recorded in silver colloid. Using Gaussian03 set of quantum chemistry codes, the vibrational wavenumber and corresponding vibrational assignments were examined theoretically. The presence of CH_2 and NO_2 bands in the SERS spectrum indicates the nearness of these groups to the metal surface, affects the orientation and metal molecule interaction. From the SERS study, it is inferred that the para substituted phenyl ring is more tilted while the tri-substituted phenyl ring assuming a nearly perpendicular orientation with respect to the metal surface. The results indicate that the B3LYP method is able to provide satisfactory results for predicting vibratiional wavenumbers and structural parameters. The calculated first hyperpolarizability is comparable with the reported values of similar derivatives. The geometrical parameters of the title compound are in agreement with that of similar derivatives.

Adsorption characteristics of naphthalene on silver are investigated using methods based on Density Functional Theory (DFT) and Surface Enhanced Raman Scattering (SERS). Vibrations in bond angles and dihedral angles of the optimized geometry of naphthalene after adsorption on silver indicate distorted hexagonal structure of the ring nearer to Ag atoms and deviation in co-planarity of carbon atoms. Theoretical computations establish binding interactions through π electron as nature bond orbital analysis confirms intermolecular charge transfers originating from the orbital overlap between π (C-C) to π*(C-C) and π (C-C) to σ*(Ag-Ag) orbitals. Higher polarization values resulting from charge transfer on adsorption, were indicated by DFT calculations, account for Raman enhancement of selective vibratiional modes and band shifts. Silver nanoparticles (AgNPs) were prepared using solution combustion method and were characterized by X-ray diffraction (XRD) and High Resolution Transmission Electron Microscopy (HRTEM). Surface Plasmon resonance peak observed around 412nm in the optical adsorption spectrum of AgNPs after adsorption of naphthalene is in good agreement with the theoretically simulated UV spectra derived using Time-Dependent Theory (TDDFT) calculation. Theoretical and experimental SERS are correlating well, strongly confirming the process of adsorption, the tilted orientation of naphthalene on silver surface and adsorption mechanism reported. Localization of electron density resulting from redistribution of electrostatic potential after adsorption on silver together with the reduction in band gap of naphthalene suggests its utility in the design of electro active organic molecular devices [112].

The FT-IR and FT-Raman spectra of 2-phenoxymethylbenzothiazole were recorded and analyzed. The Surface Enhanced Raman Scattering (SERS) spectrum was recorded in a silver colloid. The vibrational wavenumber of the compound have been computed using the Hartree-Fock/6-31G* basis and compared with the experimental values. The appearance of the Ag-O stretching mode at 237cm^{-1} in the SERS spectrum along with theoretically calculated atomic charge density, leads us to suggest that the molecule is absorbed through the oxygen atom with the molecular plane titled on the colloidal silver surface. The direction of charge transfer contribution to SERS has been discussed from the frontier orbital theory [113].

M. Anuratha et al. [114] has reported that the silver nanoparticles were synthesized using a solution combustion method with glycine as fuel. The prepared

silver nanoparticles showed an fcc crystalline structure with a particle size of 39 nm. Surface-enhanced Raman scattering (SERS) spectra of 2,3-dibromo-1,4-naphthoquinone (DBNQ) adsorbed on silver nanoparticles were investigated. The CAC stretching modes were enhanced and they were broadening in SERS spectrum with respect to normal Raman spectrum. The spectral analysis reveals that the DBNQ adsorbed flat-on orientation on the silver surface. DFT calculations were also performed to study the vibrational features of DBNQ.

M. R. Bindhu et al. [115] has investigated that the silver nanoparticles were rapidly synthesized using Moringa oleifera flower extract as the reducing agent shows surface plasmon resonance peak at 439 nm. The size and shape of the nanoparticles controlled by varying the concentration of M. oleifera flower extract in the reaction medium. The synthesized silver nanoparticles were well-dispersed spherical nanoparticles with the average size of 14 nm. The retinoic acid present in M. oleifera flower extract used as reducing agent and proteins was responsible for capping of the bioreduced silver nanoparticles. The obtained nanoparticles show size-dependent SERS activity. The SERS spectrum indicated that the pyridine adsorbed on the silver surface in a stand-on orientation via its nitrogen lone pair electrons.

M. Umadevi et al. [116] studied the size effect of silver nanoparticles on photophysical properties of 2,3-bis(chloromethyl)anthracene-1,4,9,10- tetraone (BCMAT) using an IR technique. Silver colloids of different sizes have been prepared by two different methods. Mechanisms for adsorption and complex formation have been elucidated from surface-enhanced infrared absorption spectra. The observation shows that BCMAT is adsorbed on silver nanoparticles through a C=O group and that its orientation was stand-on. Surface enhancement factors have been calculated. As the particles decrease in size their total surface area grows, which leads to the gain in the enhancement factor.

D. Arockia Jency et al. [117] reported that a highly sensitive Surface Enhanced Raman Scattering (SERS) platform for the selective trace analysis of persistent organic pollutant (POP) such as polychlorinated biphenyl (PCBs) based on β-CD modified gold nanoparticles (AuNPs) with the real environmental sample of polluted soil. The synthesized gold nanoparticles were characterized using UV-vis spectroscopy, Fourier transform infrared spectroscopy (FT-IR), X-ray diffraction

(XRD) and transmission electron microscopy (TEM). In polluted soil the presentation of PCB is confirmed by using GC-MS. It is further verified and confirmed by using SERS. When the contaminated soil was added to the system, the binding of soil with aggregation of AuNPs, and excellent Raman signal was obtained which can reflect the isomers of polychlorinated biphenyls.

The silver nanoparticles were synthesized using a solution combustion method with urea as fuel. The prepared silver nanoparticles show an FCC crystalline structure with particle size of 59 nm. FESEM image shows the prepared silver is a rod like structure. The surface-enhanced Raman scattering (SERS) spectrum indicates that the N-(1-(2-chlorophenyl)-2-(2-nitrophenyl)ethyl)-4-methylbenzenesulfonamide (CS) molecule adsorbed on the silver nanoparticles. The spectral analysis reveals that the sulfonamide is absorbed by tilted orientation on the silver surface. The Hatree Fock calculations were also performed to predict the vibrational motions of CS. This present investigation has been a model system to deduce the interaction of drugs with DNA [118].

Reference

[1] A. Sandhu, Nature Nano technol., 1 (2006) 87.

[2] D. J. Barber, I. C. Freestone, Archaeometry., 32 (1990) 33.

[3] D.D. Evanoff, G. Chumanov, Chem. Phys Chem., 6 (2005)1221.

[4] R. Feynman, Eng. Sci. Mag., 23 (1960) 22.

[5] R. Kubo, J. Phys. Soc. Jpn., 17 (1962) 975.

[6] N. Taniguchi, On the Basic Concept of Nano-Technology, Proc. Int. Con. Prod. Eng., 1974.

[7] K. Eric Drexler, Engines of creation, New York, 1986.

[8] G. Binning , H. Rohrer, C. Gerber, E. Weibel, Phys. Rev. Lett.,49 (1982) 57.

[9] G. Binning, C.F. Quate, C. Gerber, Phys. Rev. Lett., 56 (1986) 930.

[10] H. W. Kroto, J. R. Heath, S. C. Obrien, R. F. Curl, R. E. Smalley, Nature., 318 (1985) 162.

[11] S. Iijima, T. Ichihashi, Nature., 363 (1993) 603.

[12] C. A. Mirkin, T. A. Taton, Nature., 405 (2000) 626.

[13] Y. Sun, Y. Xia, Science., 298 (2002) 2176.

[14] G. Cao, Nanostructures and Nanomaterials, Imperial College Press, 2004.

[15] K. Chang, Tiny is Beautiful, Translating “Nano” into Practical, The New York Times, 2005.

[16] R. Carminati, J. J. Greffet, C. Henkel, J. M. Vigoureux, Opt. Com., 261 (2006) 368.

[17] D. A. Weitz, S. Garoff, J. I. Gersten, A. Nitzan, J. Chem. Phys., 78 (1983) 5324.

[18] H. Ditlbacher, J. R. Krenn, N. Felidj, B. Lamprecht, G. Schider, M. Salerno, A. Leitner, F.R. Aussenegg, Appl. Phys. Lett., 80 (2002) 404.

[19] G. Gece, Corros. Sci., 50 (2008) 2981.

[20] K. Fukui, Science., 218 (1987) 747

[21] D. F. V. Lewis, C. Ioannides, D. V. Parke, Xenobiotica., 24 (1994) 401.

[22] G. L. Hornyak, J. Dutta, H. F. Tibbals, A. K. Rao, Introduction to nanoscience, third ed., Taylor and Francis, New York, 2008.

[23] Y. A. Krutyakov, A. A. Kudrinskiy, A. Y. Olenin, G. V. Lisichkin, Russ. Chem. Rev., 77 (2008) 233.

[24] A. Ravindran, P. Chandran, S.S. Khan, Coll. Suff. B., 105 (2013) 342.

[25] L. Li, Y. Zhu, J. of Coll. Interf. Sci., 303 (2006) 415.

[26] M. A. El Sceyed, Acc. Chem. Res., 34 (2001) 257.
[27] D. M. K. Lam, B.W. Rossiter, Sci. Am. 265 (1991) 80.
[28] M. Q. Zhu, L. Q. Wang, J. Exarou, A. Li, J. Am. Chem. Soc., 126 (2004) 2656.
[29] J. J. Storhoff, R. Elghunian, R.W. Mucic, C. A. Mirkin, R. L. Letsinger, J. Am. Chem. Soc., 120 (1998) 1959.
[30] S. R. Nicewarner Pean, R. G. Freeman, B. D. Reiss, L. He, D. J. Pena, I. D. Walton, Science., 294 (2001) 137.
[31] L. N. Lewis, Chem. Rev., 93 (1993) 2693.
[32] H. Q. Zhao, L. Lin, J. R. Lin, J. A. Jang, M. X. Duan, L. Jiang, J. Nanoparticles. Res., 3 (2001) 321.
[33] P. V. Kamat, J. Phys. Chem. B., 106 (2002) 7729.
[34] M. P. Pileni, Adv. Funct. Mater 11(2001) 323.
[35] G. Schmid, M. Baumle, M. Bayer, Angew. Chem. Int. Ed., 39 (2009) 182.
[36] J. J. Pietron, J. F. Hicks, R.W. Murray, J. Am. Chem. Soc., 121 (1999) 5565.
[37] L. A. Dick, A. D. Mc Fatland, C. L. Haynes, R. P. Van Duyne, J. Phys. Chem. B., 106 (2002) 853.
[38] B. M. Mastiholi, V. B. Tangod, U. S. Raikar, J. Light Electron opt., 124 (2013) 261.
[39] M. M. Maye, Y. Lou, C. J. Zhong, Langmuir., 16 (2000) 7520.
[40] T. Pardeep, P. Jain, Indian Patent No. 20070608
[41] A. D. Maynard, R.J. Aitken, T. Butz, V. Colvin, K. Donaldson, water., 444 (2006) 267.
[42] E. Reichmanis, H. Katz, C. Kloc, A. Maliaka, Bell. Labs. Techn. J., 10 (2005) 87.
[43] Y. H. Chen, C. Y. Yeh, Coll. Surf. A., 197 (2002) 133.
[44] P. Rajeshwar Verma, Anti. Cancer. Agen. Med. Chem, 6 (2006) 489.
[45] A. Smekel, Naturwissenshaften, 43 (1923) 873.
[46] C. V. Raman, K. S. Krishnan, Nature., 121 (1928) 169.
[47] M. Fleischmann, P. J. Hendra, A. J. McQuillan, Chem. Phys. Lett., 26 (1974) 163.
[48] D.J. Jeanmaire, R.P. VanDuyne, J. Electro. anal. Chem., 84 (1977) 1.
[49] M. G. Albrecht, J. A. Creighton, J. Am. Chem. Soc., 99 (1977) 5215.
[50] C.V. Raman, K. S. Krishnan, Nature., 121 (1928) 501.
[51] Z. Q. Tian, B. Ren, J. F Li, Z. L Yang, Chem. Commun., 34 (2007) 3514.

[52] T. V. Dinh, Trend. Anal. Chem., 17 (1998) 558.

[53] Z. Q. Tian, J. Vib. Spectrosc., 4 (2000) 2.

[54] D.S. Wang, M. Kerker, Phys. Rev., 24, (1981) 1777.

[55] M. Kerker, J. Coll. Interf. Sci., 118 (1987) 417.

[56] C. R. Bohren, D.F. Huffman, *'Absorption and Scattering of Light by Small Particles',* John Wiley & Sons, New York (1983).

[57] F. J. Adrian, Chem. Phys. Lett., 78 (1981) 45.

[58] E. J. Zeman, G. C. Schatz, J. Phys. Chem., 91 (1987) 634.

[59] A. Campion, P. Kambhapati, Chem. Soc. Rev., 27 (1998) 241.

[60] J. De Gelder, K. De Gussem, P. Vandenabeele, L. Moens, J. Raman Spectrosc., 38 (2007) 1133.

[61] J. R. Lambardi, R. L. Birke, T. Lu, J. Xu, J. Chem. Phys., 84 (1986) 4174.

[62] H. Kneipp, I. Itzkon, R. R. Dasar, M. S. Feld, Chem. Rev., 99 (1999) 2957.

[63] M. Volkan, D. L. Stokes, T. Vo Dinh, J. Raman Spectrosc., 30 (1999) 1057.

[64] M. Moskkovits, Rev. Mod. Phys., 57 (1985) 783.

[65] S.R. Emory, S. Nie, Anal. Chem., 69 (1997) 2631.

[66] J. M. Pope, T. Sato, E. Shouji, D. A. Buttry, T. Sotomura, N. Oyama, J. Power Sources, 68 (1997) 739.

[67] S. J. Oh, K. Kim, M.S. Kim, J.Phys. Chem., 95 (1991) 8845.

[68] K. Kneipp, A. Jorio, H. Kneipp, S.D.M. Brown, K. Shafer, J. Motz, R. Satio, G. Dresselhaus, M. S. Dresselhaus, Phys. Rev., 63 (2001) 084101.

[69] A. Ruperez, J. J. Laserna, Appl. Spectrosc., 48 (1994) 219.

[70] R. L. Garrell, Anal. Chem., 61 (1980) 401.

[71] T. R. Jensen, M. D. Malinsky, C.C. Haynes, R. P. Van Duyne, J. Phys. Chem., 104 (2000) 10549.

[72] G.C. Weaver, K. Norrod, J. Chem. Ed., 75 (1998) 621.

[73] J. A. Creighton, R. J. H. Clark, R. E. Haster, Spectroscopy Surface, Wiley, Chichester, (1988).

[74] H. A. Pearce, H. Sheppard, Surf. Sci., 59 (1976) 205.

[75] R.M. Hexter, M. G. Albreccht, Spectrochiim. Acta, 35 (1978) 233.

[76] M. Moskovits, J. S. Suh, J. Phys. Chem., 88 (1984) 1293.

[77] N.V. Richardson, J. K. Sass, Chem. Phys. Lett., 62 (1979) 267.

[78] D. Zeisel, V. Deckert, R. Zenobi, T Vo Dinh, Chem. Phys. Lett., 283 (1998) 381.

[79] L. A. Dick, A. D. McFarland, C. L. Haynes, R. P. Van Duyne, J. Phys. Chem. B., 106 (2002) 853.

[80] J.A.S Gil, J.V.G. Ramos, J. Chem. Phys., 108 (1998) 317.

[81] X. Dong, H. Gu, J. Kang, X. Yuan, J. Wu, J. Mol. Struct., 984 (2010) 396.

[82] J. A. Creighton, C. G. Blatchford, M. G. Albrecht, J. Chem. Soc., 75 (1979) 790.

[83] P. C. Lee, D. Meisel, J . Phys. Chem. 86 (1979) 790.

[84] S. Sanchez Cortes, J. V. Gracia Ramos, Vib. Spectrosc., 4 (1993) 185.

[85] S. N. Emory, S. Nie, J. Phys. Chem. B., 102 (1998) 49.

[86] J. E. Pemberton, R. P. Buck, Anal. Chem., 53 (1981) 2263.

[87] B. Pettinger, U. Wenneng, H. Wetzel, Surf. Sci., 101 (1980) 409.

[88] B. H. Loo, J. Phys. Chem., 87 (1983) 3003.

[89] M. Fleishman, P. R. Graves, J. Robinson, J. Electro. Analy. Chem. 182 (1985) 87.

[90] M. M. Carraba, R. B. Edmonds, R. D. Raugh, Anal. Chem., 59 (1987) 2559.

[91] D. Thierry, C. Leygraf, Surf. Sci., 149 (1985) 592.

[92] K. D. Beer, W. Tanner, R. L. Garrell, J. Electro. Analy. Chem. 258 (1989) 313.

[93] M. Meier, A. Wokaun, T. Vo Dinh, J. Phys. Chem., 89 (1985) 1843.

[94] T. V. Dinh, M. Meier, A. Wokaun, Anal. Chim. Acta., 181 (1986) 139.

[95] C. Jennings, R. Aroca, A.M. Hor, R.O. Loutfy, Anal. Chem., 56 (1984) 2033.

[96] R. Aroca, F. Martin, J .Raman Spectrosc., 17 (1986) 243.

[97] R. P. Van Duyne, J. C. Hulteen, D.A. Treichel, J. Chem. Phys., 99 (1993) 2101.

[98] P. Aragon Santamaria, M.J. Santos Delgado, A. Maceira Vidan, L.M. Polo Diez, J.Mater.Chem., 1 (1991) 409.

[99] A.C. Pierre, Introduction to sol-gel processing, (1998), Kluwer Academic Publishers, Boston.

[100] P. Ravindranathan, S. Komarneni, R. Roy, J. Mater. Sci. Lett., 12 (1993) 369.

[101] J. J. Kingsley, L. R. Pederson, Mater. Lett., 18 (1993) 89.

[102] Y. Zhang, G. C. Stangle, J. Mater. Res., 9 (1994) 1997.

[103] E. Simth, D. Geoffrey, Modern Raman Spectroscopy-A Practical Approach, John Wiley & Sons, New York, (2005).

[104] B. Wang, D.H. Chang, G. Lu, T. H. Wang, Z.L. Zhang, Y. J. Mo, Chinese, 33 (2013) 2421.

[105] M. Umadevi, S. Jeyaseeli, M. Anuratha, P. Vanelle, T. Terme, Spectroscopy letter, 45 (2012) 438.

[106] D.Sajan, V. Bena Jothy, T. Kuruvilla, I. Hubert Joe, J. Chem. Sci, 122 (2010) 511.

[107] I. B. Cozar, L. Szabo, D. Mare, N. Leopold, L. David, V. Chis, J. Molecular. Structure, 993 (2011) 243.

[108] Y. Sheena Mary, L. Ushakumari, B. Harikumar, H. Tresa Varghese, C. Yohannan Panicker, J. Iran. Chem. Soc., 6 (2009) 138.

[109] P.L. Anto, R. J. Anto, H.T. Varghese, C.Y. Panicker, D. Philip, A.G. Brolo, J. Raman. Spectrosc, 40 (2009) 1810.

[110] H. Tresa Varghese, C. Yohannan Philip, K. Sreevalsan, V. Anithakumary, Spectr. Chimi. Acta Part A., 68 (2007) 817.

[111] Y. Sheena Mary, K. Raju, T. Ertan Bolelli, I. Yildiz, H.I.S. Nogueira, C. M. Granadeiro , C. Van Alseony, J. Mole. Struct., 1012 (2012) 22.

[112] T. N. Rekha, M. Umadevi, B. J. M. Rajkumar, J. Mole. Strut., 1079 (2015)155.

[113] C. Yohannan Panicker, H. Tresa Varghese, A. Raj, K. Raju, T. Ertan Bolelli, I. Yildiz, O. Temiz Arpaci, C. M. Granadeiro, H. I. S. Nogueria, Spectr. Chimi. Acta Part A., 74 (2009) 132.

[114] M. Anuratha, Jawahar, M. Umadevi, V.G. Sathe, P. Vanelle, T. Terme, V. Meenakumari, Milton Franklin Benial, Spectr. Chimi. Acta Part A., 105 (2013) 218.

[115] M. R. Bindhu, V. Sathe, M. Umadevi, Spectr. Chimi. Acta Part A., 115 (2013) 409.

[116] M. Umadevi, P. Vanelle, T. Termeb, J. Appl. Spectrosc., 79 (2012) 189.

[117] D. Arockia Jency, M. Umadevi, G.V. Sathe, J. Raman Spectrosc, (2015) DOI 10.1002/jrs.4654.

[118] M. Anuratha, A. Jawahar, M. Umadevi, V.G. Sathe, P. Vanelle, T. Terme, V. Meenakumari, A. Milton Franklin Benial Spectr. Chimi. Acta Part A., 131 (2014) 261.

Figure 1.1 Roman Lycurgus bronze cup at the British Museum, lit from the outside (left) and from the inside (right).

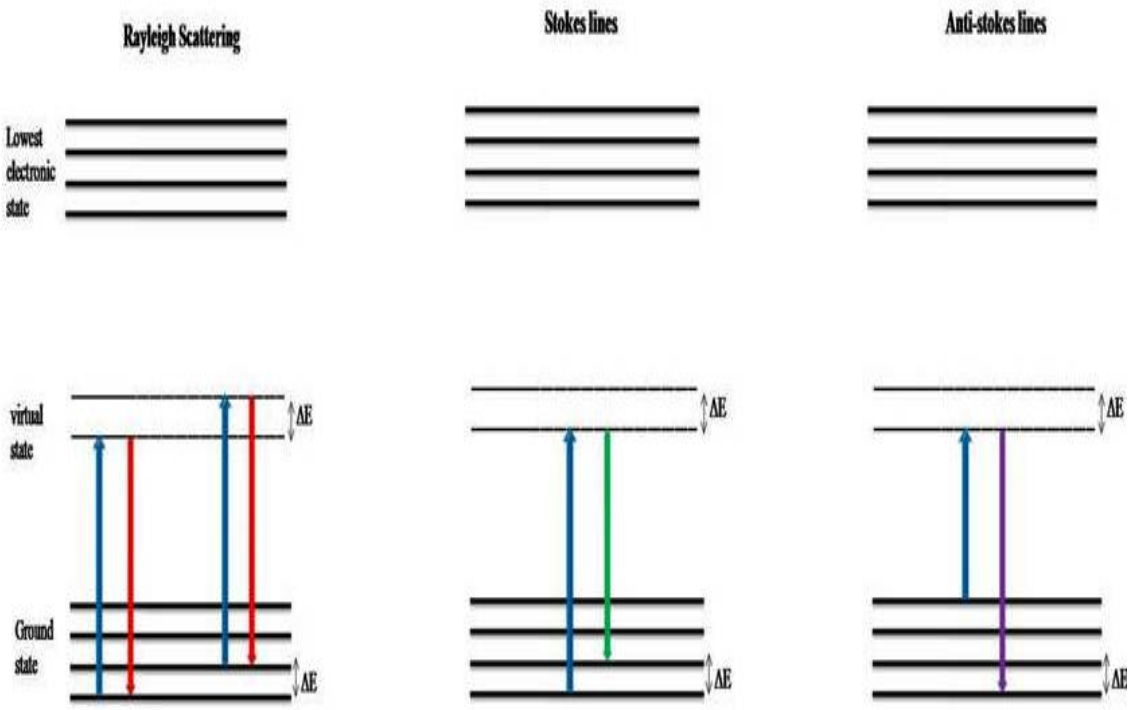

Figure 1.2 The quantum image for different case of scattering.

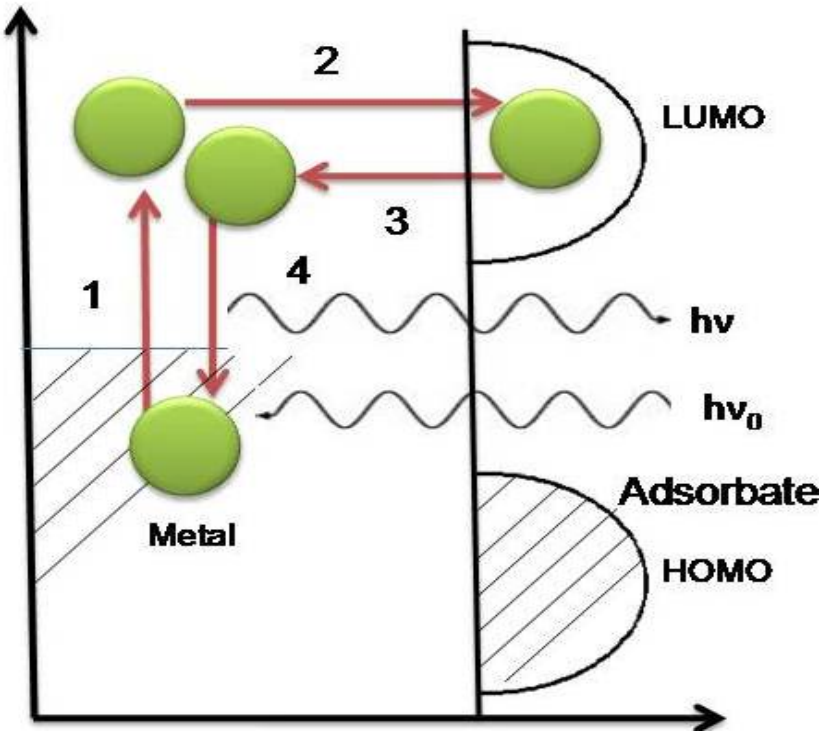

Figure 1.3 Schematic diagram of the four-step process of the photon-driven charge transfer model for a molecule adsorbed on an electrode.

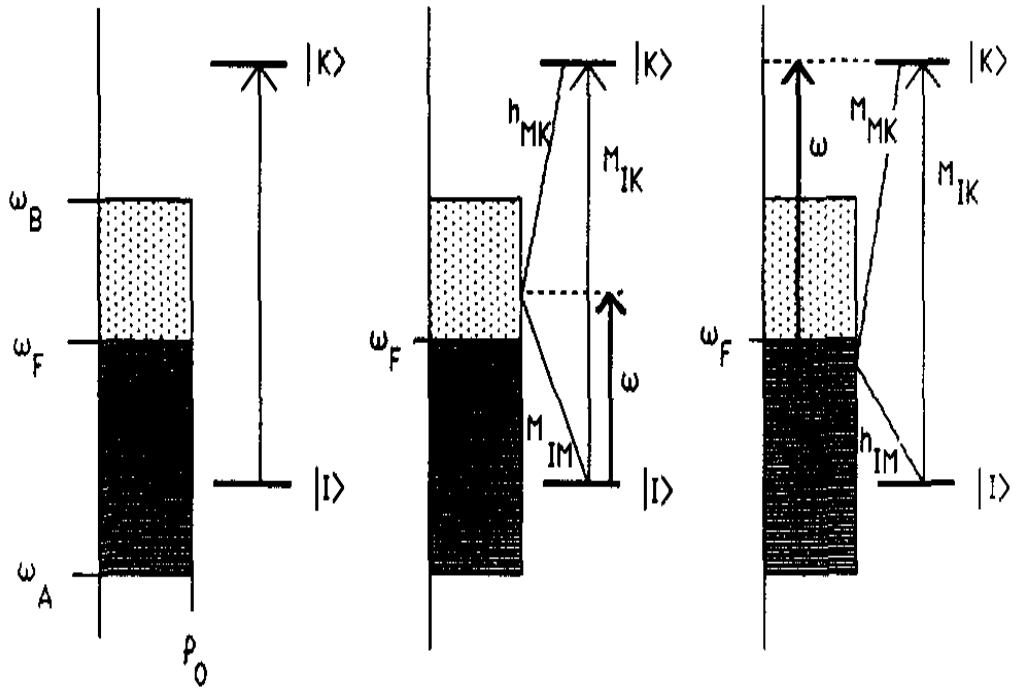

Figure 1.4 a) Energy level diagram for molecule to metal system (lines-filled levels; dots-unfilled levels) b) Molecule to metal charge transfer transitions and c) Metal to molecule charge transfer transitions.